J. Appl. Comput. Mech., 11(4) (2025) 1022-1038
DOI: 10.22055/jacm.2024.47914.4837

ISSN: 2383-4536
jacm.scu.ac.ir

Shahid Chamran
University of Ahvaz

Journal of
Applied and Computational Mechanics

Research Paper

Optimal Frequency of Stiffened Piezolaminated Composite Plates Implementing a Hybrid Special Relativity Search and Hill Climbing Optimization Algorithm

Vahid Goodarzimehr[1], Umut Topal[2], Mehdi Bohlooly Fotovat[3]

[1] Department of Civil Engineering, Shahid Chamran University of Ahvaz, Ahvaz, Iran, Email: v.goodarzimehr@scu.ac.ir

[2] Department of Civil Engineering, Karadeniz Technical University, Trabzon, Turkey, Email: utopal@ktu.edu.tr

[3] Department of Strength of Materials, Lodz University of Technology, Stefanowskiego 1/15, 90-537 Lodz, Poland, Email: mehdi.bohlooly-fotovat@p.lodz.pl

Received September 12 2024; Revised October 29 2024; Accepted for publication December 30 2024.
Corresponding author: V. Goodarzimehr (v.goodarzimehr@scu.ac.ir)

Abstract. This study focuses on maximizing the fundamental frequency of stiffened piezolaminated composite plates using a novel hybrid optimization algorithm that combines the Special Relativity Search (SRS) and Hill Climbing (HC) techniques. The optimization process maximizes the fundamental frequency by adjusting the fiber orientations within the composite layers. The mathematical models, based on Classical Laminated Plate Theory (CLPT) are solved using MATLAB. The impact of various parameters, including boundary conditions, grid shapes, angles of diagonal ribs, and plate aspect ratios, on the optimized frequency results is thoroughly examined. The results demonstrate that the SRSHC algorithm outperforms the Special Relativity Search (SRS) algorithm, confirming its effectiveness in complex optimization problems with large search spaces. This research contributes to advancing the design of smart structures with enhanced dynamic performance.

Keywords: Stiffened piezolaminated plate; Frequency; Optimization; Special Relativity Search based on Hill Climbing algorithm, SRS Algorithm.

1. Introduction

Piezoelectric materials are frequently utilized to design the intelligent and smart structures with bonded or embedded sensors/actuators in many disciplines such as civil, marine, automotive, mechanical, aerospace, and nuclear engineering. These materials are employed to efficiently suppress the free vibration, forced vibration, and snap-through phenomenon or to control the buckling, deflection, stress, post-buckling deflection, and shape of the structure.

Numerous studies have investigated the vibration behavior of piezolaminated plates, focusing on different aspects such as nonlinear and linear vibrations, numerical and finite element methods, advanced control methods, optimization strategies, and thermal effects. This review categorizes these studies based on the specific objectives addressed in the research. Nonlinear vibration analysis of piezolaminated plates has been an area of significant research interest, particularly in understanding complex behaviors under different loading conditions. Jayakumar et al. [1] examined nonlinear vibrations using von-Karman's equations for plates integrated with actuators and sensors. Similarly, Panda and Ray [2] addressed the nonlinear dynamic response of piezolaminated plates using the first-order shear deformation theory, while Dash and Singh [3, 4] investigated nonlinear vibrations using higher-order shear deformation theory, aiming to improve accuracy for thicker plates. Huang and Shen [5] extended this analysis by focusing on cross-ply configurations and considering the combined effects of electrical, thermal, and mechanical loads through von-Karman-type equations. Furthering this line of work, Deepak et al. [6] examined the nonlinear free vibration behavior under thermo-piezoelectric loads, employing von Karman nonlinearity for better accuracy. Zhang et al. [7] explored chaotic motion and nonlinear vibration in cross-ply symmetric plates, providing insights into transverse and in-plane loading effects. Moita et al. [8] conducted a comprehensive nonlinear analysis based on the classical laminated plate theory (CLPT), integrating actuators and sensors for enhanced dynamic performance.

Linear vibration analysis, as well as the development of efficient plate models, has been crucial for simplifying vibration studies in certain applications. Krommer [9] presented a linear analysis for piezolaminated plates, applying a unique modeling approach to study fundamental vibration behaviors. Shu [10] developed a model specifically for cylindrical bending of piezolaminated plates, offering a more focused approach to certain structural applications. Pietrzakowski [11] utilized Kirchhoff's hypothesis to develop a model that incorporates piezoelectric sensors and actuators, simplifying the vibration analysis for thin plates. Milazzo and Orlando

Published online: January 05 2025

[12] proposed an equivalent single-layer model to further streamline the vibration analysis of piezolaminated plates, contributing to computational efficiency.

Finite element methods and other numerical techniques have been extensively applied to understand and predict the vibration behavior of piezolaminated plates under various conditions. Akhras and Li [13] developed a spline finite strip method, providing a foundation for vibration solutions in piezolaminated structures. Torres and Mendonça [14] improved upon existing hybrid models, enhancing formulation accuracy for plates with integrated actuators and sensors. Topdar et al. [15] presented a refined hybrid plate model for vibration analysis, which accounts for detailed structural characteristics. Loja et al. [16] introduced a higher-order B-spline finite strip method specifically for laminated plates, offering higher accuracy in vibration predictions. Chanda et al. [17] incorporated foundations into their finite element solutions, analyzing both controlled and uncontrolled vibrations of piezolaminated plates. Robaldo et al. [18] applied the principle of virtual displacements to create a combined finite element formulation, while Tanzadeh and Amoushahi [19] extended finite strip techniques to handle complex vibration scenarios in piezolaminated plates. Zhang et al. [20] implemented the differential quadrature technique for vibration analysis, showcasing its potential for accuracy in vibration predictions. Phung-Van et al. [21] proposed a straightforward and effective finite element formulation to support dynamic control in vibration analysis for plates with sensors and actuators.

Advanced vibration control methods have been developed to enhance the stability and performance of piezolaminated plates. Jiang et al. [22] utilized a method of positive position feedback control to achieve nonlinear vibration suppression, demonstrating its potential for active control in dynamic applications. Lu et al. [23] introduced a control strategy designed for plates subjected to aerodynamic loads within a hygro-thermal environment, addressing complex operational conditions. Talebitooti et al. [24] employed the element-free Galerkin technique for both vibration control and shape analysis, highlighting its flexibility in dealing with irregular geometries. Oh et al. [25] studied vibrations in partially eccentric and fully symmetric piezolaminated plates, taking into account large thermopiezoelastic deflections to refine the control approach. Donadon et al. [26] experimentally and numerically investigated the effects of piezoelectric excitation on frequency variations, offering insights into frequency tuning for vibration control.

Mesh-free and isogeometric methods have provided alternative approaches to conventional finite element analysis, enhancing flexibility and accuracy in complex scenarios. Momeni and Fallah [27] proposed a mesh-free finite-volume approach, demonstrating its effectiveness in investigating plate vibrations without the limitations of mesh dependency. Nguyen-Quang et al. [28] introduced an isogeometric approach to study the dynamic response of piezolaminated plates, which allows for smooth representation of complex geometries and can potentially improve accuracy over traditional finite element methods.

While extensive research has been conducted on vibration analysis, fewer studies focus on frequency optimization and design improvements in piezolaminated plates. Niu et al. [29] addressed this gap by applying discrete material optimization to minimize the dynamic response of piezolaminated plates. Correia et al. [30, 31] utilized stochastic global optimization and multiobjective optimization approaches to maximize the natural frequencies, minimize elastic strain energy, and enhance buckling load in their designs. Padoin et al. [32] developed a topology optimization strategy to control structural vibrations through a linear-quadratic optimal control method, offering a novel approach to manage external perturbations. Alamir [33] investigated optimal control and design strategies, contributing insights into improving performance through optimized structural configurations. Temperature-dependent vibration analysis is critical for applications in thermal environments, where temperature variations can significantly impact plate dynamics. Li et al. [34] proposed a real-time temperature feedback strategy for analyzing the vibration response of sandwich piezolaminated plates, providing a methodology to handle temperature effects in practical applications. Goodarzimehr et al. [35, 36] presented new methods based on metaheuristic algorithms for optimizing complex problems in modern materials engineering. By maximizing buckling resistance and structural frequency in two stages, they successfully improved the performance of laminated structures across various industrial applications. The optimization of structural engineering problems, including discrete structures, geometric nonlinear structures, and dynamic analysis and design, represents other complex engineering challenges that cannot be solved using classical methods. Goodarzimehr et al. [37-39] developed three new methods based on the crowd intelligence algorithm, all of which achieved better results compared to previous approaches. Omidi Nasab and Goodarzimehr [40] proposed a novel hybrid method for optimizing the weight of truss structures. Zarzoor et al. [41] enhanced the efficiency of wind turbine structures by improving their dynamic performance. Inman and Gunasekar [42] introduced a method for classifying structural frequencies using the inverse approach.

Based on the above literature view and to the best of our knowledge, there is no research study about the frequency optimization of stiffened piezolaminated plates. Therefore, this research aims to fill the gap in the literature. This paper investigates frequency optimization of stiffened piezolaminated plates using SRSHC algorithm. The fundamental frequency is maximized by optimizing the fiber orientations in the layers. The constitutive equations are discretized via CLPT. The optimization results are presented for different boundary conditions, grid shapes, angle of the diagonal ribs, and plate aspect ratios.

The remainder of this paper is organized as follows: Section 2 presents the fundamental equations and mechanical modeling for stiffened piezolaminated composite plates based on the classical laminated plate theory (CLPT). In Section 3, the hybrid optimization algorithm, combining Special Relativity Search (SRS) and Hill Climbing (HC), is introduced, along with its theoretical basis and implementation. Section 4 outlines the formulation of the optimization problem, specifying design variables and objective functions. Section 5 provides a detailed report on the numerical experiments conducted to validate the proposed method. In Section 6, the optimization results are presented, analyzing the impact of various parameters such as boundary conditions, grid shapes, and aspect ratios on the optimized frequency. Finally, Section 7 concludes the paper with a discussion of key findings, implications for composite plate design, and future research directions.

2. Basic Equations

Figure 1(a) shows the coordinate system and geometry of a stiffened piezolaminated plate. The length, width, and thickness of the plate are $2a$, $2b$ and h, respectively. The plate is composed of a multilayered composite substrate, two piezoelectric layers adhered to the bottom and top surfaces of the plate and a concentric stiffener. h_a, h_c, and h_s are the thickness of the composite layer, piezoelectric layer, and stiffener, respectively. It is supposed that four edges of the middle-plane of the plate are supported by two types of springs, i.e., linear (l), and rotational (r). By choosing zero or substantial values of the stiffness of these springs $k_i^l, k_i^r \ (i = 1,...,4)$, one can model free (F), clamped (C), and simply supported (S) edge conditions. This study considers five different grid shapes such as angle grid, ortho grid, iso grid1, orthotropic grid, and iso grid2 for stiffener (Fig. 1(b)). In Fig. 1(c), schematic view of an orthotropic grid can be seen. Here, d_{11s}, d_{22s}, and d_{12s} are the width of the transverse, longitudinal, and diagonal ribs, respectively; S_{11s}, S_{22s} and S_{12s} are the span between two parallel transverse, longitudinal, and diagonal ribs, respectively. The angle of the diagonal ribs (ϕ) is measured from the x-axis.

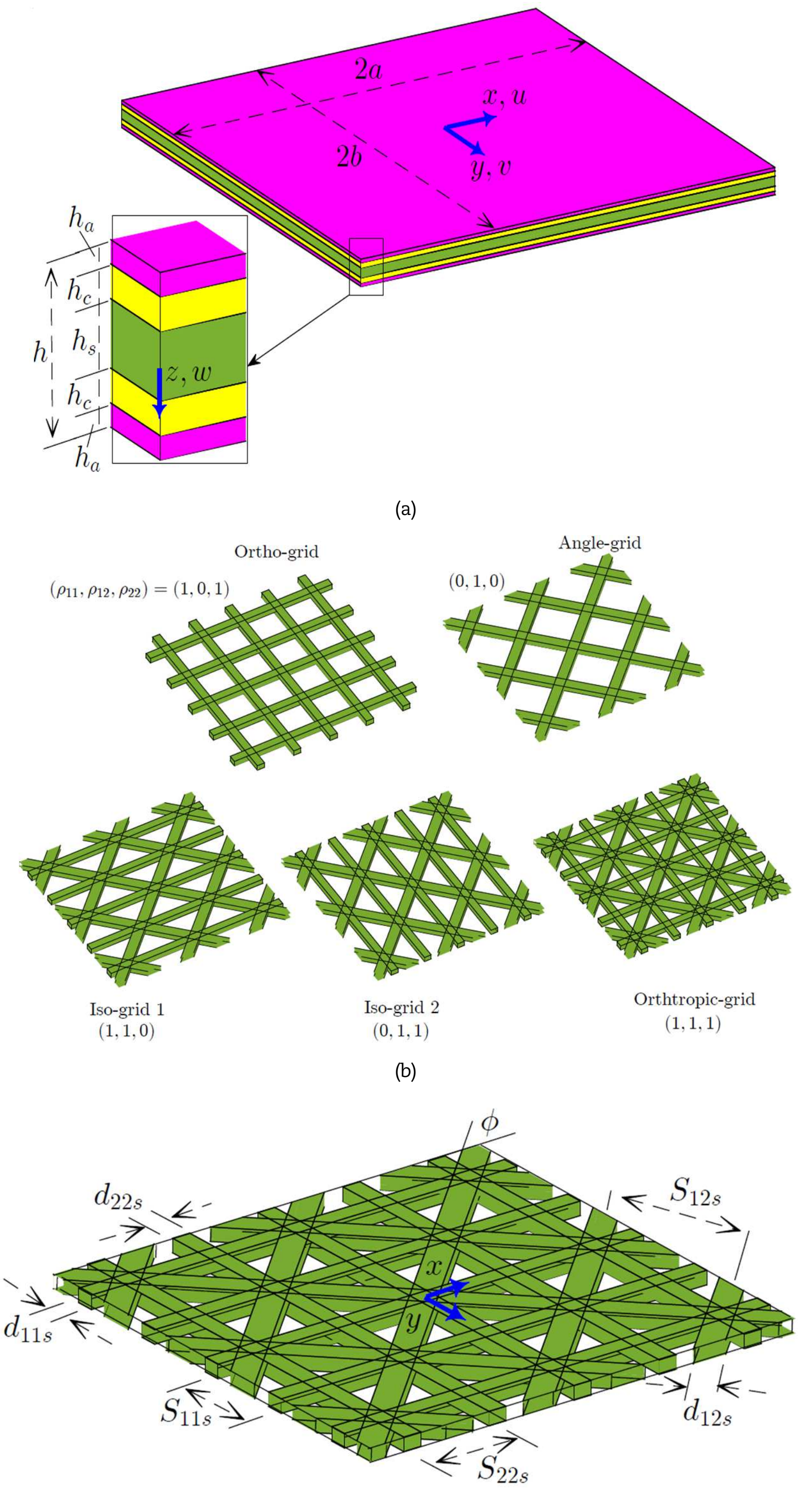

Fig. 1. (a) Coordinate system and geometry parameters of a stiffened piezolaminated plate, (b) Five different grid shapes, and (c) Schematic view of an orthotropic grid.

According to CLPT, the displacement fields can be written as:

$$\begin{aligned} u(x,y,z,t) &= u_0(x,y,t) - z \,.\, W_{0,x}(x,y,t) \\ V(x,y,z,t) &= V_0(x.y.t) - z \cdot W_{0,y}(x,y,t) \\ W(x,y,z,t) &= W_0(x,y,t) \end{aligned} \tag{1}$$

where, u_o, V_o, and W_o are the displacements in the plate midplane. The strains can be written as:

$$\varepsilon = \varepsilon^o + ZK \tag{2}$$

where, the strain ε^o at the mid-plane based on von Karman's strain-displacement relationship is:

$$\varepsilon^o = \begin{Bmatrix} \varepsilon_x^o \\ \varepsilon_y^o \\ \gamma_{xy}^o \end{Bmatrix} = \begin{Bmatrix} u_{o,x} + \frac{1}{2}W_{o,x}^2 \\ V_{o,y} + \frac{1}{2}W_{o,y}^2 \\ u_{o,y} + V_{o,x} + W_{o,x}W_{o,y} \end{Bmatrix} \tag{3}$$

However, the nonlinear terms in Eq. (3) can be omitted for linear analysis and the curvature k is defined as:

$$K = \begin{Bmatrix} K_x \\ K_y \\ K_{xy} \end{Bmatrix} = \begin{Bmatrix} -W_{o,xx} \\ -W_{o,yy} \\ -2W_{o,xy} \end{Bmatrix} \tag{4}$$

With the consideration of the electrical load, the stress-strain relationship of a piezoelectric actuator is given below:

$$\begin{Bmatrix} \sigma_x \\ \sigma_y \\ \tau_{xy} \end{Bmatrix} = \begin{pmatrix} Q_{11}^a & Q_{12}^a & 0 \\ Q_{21}^a & Q_{22}^a & 0 \\ 0 & 0 & Q_{66}^a \end{pmatrix} \begin{Bmatrix} \varepsilon_x \\ \varepsilon_y \\ \gamma_{xy} \end{Bmatrix} - \begin{pmatrix} 0 & 0 & e_{31} \\ 0 & 0 & a_{23} \\ 0 & 0 & 0 \end{pmatrix} \begin{Bmatrix} E_x \\ E_y \\ E_z \end{Bmatrix} \tag{5}$$

where $Q_{ij}^a (i,j = 1,2,6)$ are the elastic stiffness; (e_{31}, e_{32}) are the piezoelectric stiffness, and (E_x, E_y, E_z) are the applied electric field components. For the k^{th} orthotropic lamina, the stress–strain relationship can be defined as:

$$\begin{Bmatrix} \sigma_x \\ \sigma_y \\ \tau_{xy} \end{Bmatrix} = \begin{pmatrix} \overline{Q_{11}} & \overline{Q_{12}} & \overline{Q_{16}} \\ \overline{Q_{21}} & \overline{Q_{22}} & \overline{Q_{26}} \\ \overline{Q_{61}} & \overline{Q_{62}} & \overline{Q_{66}} \end{pmatrix} \begin{Bmatrix} \varepsilon_x \\ \varepsilon_y \\ \gamma_{xy} \end{Bmatrix} \tag{6}$$

where $\overline{Q}_{ij}$ are the transformed stiffness. The stress–strain relationship for the stiffener can be defined as follows [43-45]:

$$\begin{Bmatrix} \sigma_x \\ \sigma_y \\ \tau_{xy} \end{Bmatrix} = \begin{pmatrix} \rho d_{11s} E_S/S_{11S} + 2\lambda d_{12s} E_S c^4/S_{12S} & 2\lambda d_{12s} E_s c^2 s^2/S_{12s} & 0 \\ 2\lambda d_{12s} E_s c^2 s^2/S_{12s} & \psi d_{22s} E_s/S_{22s} + 2\lambda d_{12s} E_s s^4/S_{12s} & 0 \\ 0 & 0 & 2\lambda d_{12s} E_s c^2 s^2/S_{12s} \end{pmatrix} \begin{Bmatrix} \varepsilon_x \\ \varepsilon_y \\ \gamma_{xy} \end{Bmatrix} \tag{7}$$

where c = $\cos\theta$, s = $\sin\theta$, and E_s is the Young's modulus of the stiffener. (ρ, ψ, λ) are defined in Fig. 1(b) for five different grid shapes. The force N and moment M resultants can be obtained as:

$$N = \begin{Bmatrix} N_x \\ N_y \\ N_{xy} \end{Bmatrix} = \begin{pmatrix} A^*_{11} & A^*_{12} & A^*_{16} \\ A^*_{21} & A^*_{22} & A^*_{26} \\ A^*_{61} & A^*_{62} & A^*_{66} \end{pmatrix} \begin{Bmatrix} \varepsilon_x^0 \\ \varepsilon_y^0 \\ \gamma_{xy}^0 \end{Bmatrix} - \begin{pmatrix} A_{11}^a & A_{12}^a & A_{16}^a \\ A_{21}^a & A_{22}^a & A_{26}^a \\ A_{61}^a & A_{62}^a & A_{66}^a \end{pmatrix} \begin{Bmatrix} d_{31} \\ d_{32} \\ 0 \end{Bmatrix} \tag{8}$$

$$M = \begin{Bmatrix} M_x \\ M_y \\ M_{xy} \end{Bmatrix} = \begin{pmatrix} D^*_{11} & D^*_{12} & D^*_{16} \\ D^*_{21} & D^*_{22} & D^*_{26} \\ D^*_{61} & D^*_{62} & D^*_{66} \end{pmatrix} \begin{Bmatrix} K_x \\ K_y \\ K_{xy} \end{Bmatrix} \tag{9}$$

where d_{31} and d_{32} are the dielectric constants of the piezoelectric actuators and:

$$\begin{aligned} A^* = \begin{pmatrix} A^*_{11} & A^*_{12} & A^*_{16} \\ A^*_{21} & A^*_{22} & A^*_{26} \\ A^*_{61} & A^*_{62} & A^*_{66} \end{pmatrix} &= \begin{pmatrix} Q_{11}^a & Q_{12}^a & 0 \\ Q_{21}^a & Q_{22}^a & 0 \\ 0 & 0 & Q_{66}^a \end{pmatrix} I_1^a + \\ &\begin{pmatrix} \rho d_{11s} E_S/S_{11S} + 2\lambda d_{12s} E_S c^4/S_{12S} & 2\lambda d_{12s} E_s c^2 s^2/S_{12s} & 0 \\ 2\lambda d_{12s} E_s c^2 s^2/S_{12s} & \psi d_{22s} E_s/S_{22s} + 2\lambda d_{12s} E_s s^4/S_{12s} & 0 \\ 0 & 0 & 2\lambda d_{12s} E_s c^2 s^2/S_{12s} \end{pmatrix} I_1^s + \begin{pmatrix} A_{11} & A_{12} & A_{16} \\ A_{21} & A_{22} & A_{26} \\ A_{61} & A_{62} & A_{66} \end{pmatrix} \end{aligned} \tag{10}$$

$$A^a = \begin{pmatrix} A_{11}^a & A_{12}^a & A_{16}^a \\ A_{21}^a & A_{22}^a & A_{26}^a \\ A_{61}^a & A_{62}^a & A_{66}^a \end{pmatrix} = \begin{pmatrix} Q_{11}^a & Q_{12}^a & 0 \\ Q_{21}^a & Q_{22}^a & 0 \\ 0 & 0 & Q_{66}^a \end{pmatrix} E_z I_1^a \tag{11}$$

$$\begin{aligned} D^* = \begin{pmatrix} D^*_{11} & D^*_{12} & D^*_{16} \\ D^*_{21} & D^*_{22} & D^*_{26} \\ D^*_{61} & D^*_{62} & D^*_{66} \end{pmatrix} &= \begin{pmatrix} Q_{11}^a & Q_{12}^a & 0 \\ Q_{21}^a & Q_{22}^a & 0 \\ 0 & 0 & Q_{66}^a \end{pmatrix} I_3^a \\ &+ \begin{pmatrix} \rho d_{11s} E_S/S_{11S} + 2\lambda d_{12s} E_S c^4/S_{12S} & 2\lambda d_{12s} E_s c^2 s^2/S_{12s} & 0 \\ 2\lambda d_{12s} E_s c^2 s^2/S_{12s} & \psi d_{22s} E_s/S_{22s} + 2\lambda d_{12s} E_s s^4/S_{12s} & 0 \\ 0 & 0 & 2\lambda d_{12s} E_s c^2 s^2/S_{12s} \end{pmatrix} I_3^s + \begin{pmatrix} D_{11} & D_{12} & D_{16} \\ D_{21} & D_{22} & D_{26} \\ D_{61} & D_{62} & D_{66} \end{pmatrix} \end{aligned} \tag{12}$$

where,

$$I_1^a = 2h_a, I_1^s = h_s, I_3^a = 2h_c^2 h_a + 2h_c h_a^2 + \frac{3}{2}h_a^3 + \frac{1}{2}h_a h_s^3, I_3^s = h_c^2 h_s + 2h_c h_a h_s + h_a^2 h_c + \frac{1}{12}h_s^3 \tag{13}$$

In Eqs. (10) and (12), A_{ij} and D_{ij} are the extensional and bending stiffnesses of the laminates, respectively, and they are defined as:

$$A_{ij}, D_{ij} = \sum_{k=1}^{n} \begin{pmatrix} \overline{Q_{11}} & \overline{Q_{12}} & 0 \\ \overline{Q_{21}} & \overline{Q_{22}} & 0 \\ 0 & 0 & \overline{Q_{33}} \end{pmatrix} \left\{ (Z_K - Z_{K-1}), \frac{1}{3}(Z_K^3 - Z_{K-1}^3) \right\} \quad i,j = 1,2,6 \tag{14}$$

and the extension-bending coupling matrix is zero due to symmetric layer arrangement. The total potential energy Π of the plate can be defined as follows:

$$\Pi = U - V + T + \sum_{i=1}^{4} \psi_i + \sum_{i=1}^{4} \Upsilon_i \tag{15}$$

where i = 1,2,3 and 4 denotes edges $x = -a$, $x = a$, $y = -b$, and $y = b$, respectively. The definition of saved energy in these springs can be find in [43-45].

The strain energy U, the potential energy by the external forces V, and the kinetic energy T of the plate are given by:

$$U = \frac{1}{2}\iiint (\sigma_x \varepsilon_x + \sigma_y \varepsilon_y + \tau_{xy}\gamma_{xy})dxdydz \tag{16}$$

$$V = \iint \left[\frac{1}{b}P_x u_x + \frac{1}{a}P_y v_y \right] \tag{17}$$

$$T = \iiint \rho \left\{ (\frac{\partial u}{\widehat{ct}})^2 + (\frac{\partial v}{\widehat{ct}})^2 + (\frac{\partial w}{\widehat{ct}})^2 \right\} dxdydz \tag{18}$$

In Eq. (15), ψ_i and Υ_i are the strain energy of the linear and rotational springs for different edges, respectively. In Eq. (17), P_x and P_y are the compressive forces applied to the edges of the plate in the x and y directions, respectively. However, it is assumed that there is no compressive load. So, it will be zero. By substituting kinetic and strain energies into Lagrange equation [46], the linear equations of motions can be found.

In this study, all edges are assumed to be free, and the spring factors determines the edge conditions. As a results, there is no constraint to be satisfied, and a unified deflection function satisfies all possible boundary conditions. Based on Ritz method, displacement function contains an unknown set of the coefficients C_{mn} as follows:

$$w = \sum_{m=0}^{M}\sum_{n=0}^{N} C_{mn} \varsigma^m \eta^n \tag{19}$$

where $\varsigma = x/a$, $\eta = y/b$, M and N are the numbers of the terms in the admissible functions. With respect to the Ritz method, substitute Eq. (16) and (18) into Eq. (15), then minimize Π in accordance with the unknown coefficients C_{mn}:

$$\frac{\partial \Pi}{\partial C_{mn}} = 0 \quad m = 0,1,\ldots,M \quad n = 0,1,\ldots,N \tag{20}$$

The above differentiations yield to the (M+1).(N+1) equations. By rewriting them as a vector form, one can obtain:

$$[\overline{M}]\ddot{q} + [\overline{K}]q = 0 \tag{21}$$

where $[\overline{K}]$ and $[\overline{M}]$ are the stiffness and mass matrices, respectively. In Eq. (21), displacement and acceleration vectors can be written as:

$$\ddot{q} = [\ddot{C}_{00}, \ddot{C}_{01}, \ldots, \ddot{C}_{0N}, \ldots, \ddot{C}_{MN}]^T \tag{22}$$

$$q = [C_{00}, C_{01}, \ldots, C_{0N}, \ldots, C_{MN}]^T \tag{23}$$

By assuming a periodic motion of the deflection $(C_{mn} = \overline{C}_{mn} e^{i\omega t})$, Eq. (21) can be rewritten as:

$$[\overline{K} - \omega^2 \overline{M}]q = 0 \tag{24}$$

where ω is the eigen-value or natural frequency and the lowest of the frequency is the fundamental frequency of stiffened piezolaminated plate. Additionally, the mode shape of the structure based on different natural frequencies can be obtained using eigen-vectors of each eigen-values in Eq. (24). Figure 2 shows the procedure for solving the problem.

3. Special Relativity Search (SRS) Algorithm

SRS algorithm was first introduced by Goodarzimehr et al. [47] and Goodarzimehr et al. [48]. This algorithm simulates the collective motion process of particles in a magnetic field. However, the equations of the SRS algorithm were formulated based on the special relativity physics. In this way, the particles exert force on each other and this force creates the movement towards the optimal response.

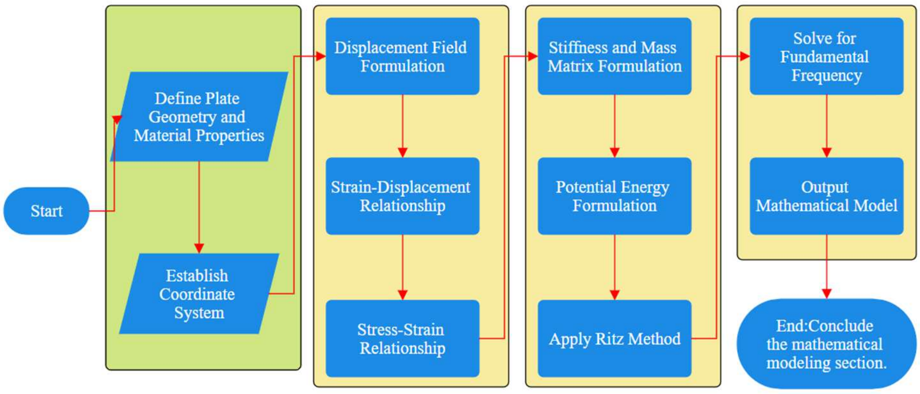

Fig. 2. Procedure for solving the frequency of stiffened piezolaminated plate.

This algorithm starts the search operation with a random point in the search space using the concept of the SRS. One of the significant features of the SRS algorithm is that it seeks the local optimums sufficiently close to the global optimum to improve the optimization. This idea can be very effective in improving the optimization performance in complex problems with large search spaces. The various stages and formulations of this algorithm are described as follows:

***Search Space*:** The search space is defined using Eq. (25):

$$X_{i,j} = \begin{bmatrix} \mathbf{X}_{1,1} & \mathbf{X}_{1,2} & & \mathbf{X}_{1,j} \\ \mathbf{X}_{2,1} & \mathbf{X}_{2,1} & & \mathbf{X}_{2,1} \\ \vdots & \vdots & \ddots & \\ \vdots & \vdots & & \\ \mathbf{X}_{i,1} & \mathbf{X}_{i,2} & & \mathbf{X}_{i,j} \end{bmatrix} \tag{25}$$

$$X_i \in [X_{min}, X_{max}] \tag{26}$$

where X_i is the vector of input variables for the i^{th} row, X_{min} and X_{max} are the minimum and maximum feasible values for the variable X_i, respectively. The SRS algorithm requires a random point to start the optimization process. Equation (27) is used for generating a random point from the feasible space:

$$X_i = X_{min} + rand(0,1).(X_{max} - X_{min}) \tag{27}$$

***Objective Function*:** After generating design variables, objective function must be calculated. After calculating objective function, the best and worst values of objective function are identified. Objective function is expressed using Eq. (28):

$$Fitness_i = ObjectiveFunction(X_i) \tag{28}$$

where fitness indicates the output of objective function calculated in the i^{th} iteration.

Main loop of SRS algorithm: In SRS algorithm, first, the positions of two particles, X_i, X_j, in search space are determined. Then, using Eq. (29), the distance between two particles is calculated using the Euclidean norm:

$$R_{ij}^t = \frac{norm\left(pos_i^t - pos_j^t\right)}{pos_i^t + pos_j^t} \tag{29}$$

where X_i^t and X_j^t represent the positions of the i^{th} and j^{th} particles in the t^{th} iteration, respectively. R_{ij}^t is the distance between two particles in the search space.

The charge of the particles in a magnetic field can be determined by calculating Lorentz force. This force is proportional to the charge of the particle, the velocity of the particle, and the intensity of the magnetic field. The Lorentz law is used to calculate this force and, consequently, the charge of the particles in the magnetic field. In this research, an empirical equation is proposed for calculating the charge of particles. Equations (30) and (31) are employed for modeling the charge of the particles. Using the *Best*, *Worst*, and *cost*, the charge of the particles can be calculated instantaneously. In fact, these equations indicate that the greater the charge of the particles, the more guaranteed the dynamic nature of the particle movement will be obtained:

$$Q_i^t = \frac{cost_i - Best}{Worst - Best} \tag{30}$$

$$Q_j^t = \frac{cost_j - Best}{Worst - Best} \tag{31}$$

where Q_i and Q_j are the charges of the i^{th} and j^{th} particles in the t^{th} iteration, respectively; $cost_i$ and $cost_j$ are the outputs of the objective function for the i^{th} and j^{th}, respectively, *Best* and *Worst* are the maximum and minimum values of the objective function, respectively.

At this stage, we must calculate the velocity of particles in a magnetic field. To calculate the velocity of particles in a magnetic field, the Lorentz motion equations are used. The Lorentz motion equations for a particle with charge Q and velocity V moving in a magnetic field with intensity B are as follows:

$$\vec{F} = Q(\vec{V} \times \vec{B}) \tag{32}$$

$$\vec{F} = m\vec{a} \tag{33}$$

where $\bar{F}$ is the Lorentz force; Q is the charge of the particle; V is the velocity of the particle; $\vec{B}$ is the intensity of the magnetic field; m is the mass of the particle, and $\vec{a}$ is the acceleration of the particle, respectively.

Using above equations, the value of velocity in new direction can be calculated. For this purpose, first, Eq. (32) must be equated with Eq. (33) to obtain the acceleration. Then, by integrating or solving the differential of Eq. (33), the velocity of the particle is calculated. By substituting the values of the magnetic field and charge and performing a series of simplifications, the value of the velocity of the particle is calculated using Eq. (34):

$$V_i^t = \frac{Xi - Xj}{\Delta t} \tag{34}$$

The motion of particles in a magnetic field depends on several factors, including the angular frequency. Therefore, it is necessary to develop a new equation to calculate angular frequency. To calculate frequency of motion of charged particles in a magnetic field, Cyclotron Resonance or Gyllen-Lewis equation is applied as given Eq. (35):

$$f = \frac{qB}{2\pi m} \tag{35}$$

$$\omega = 2\pi f = \frac{QB}{m} \tag{36}$$

with substitution B, Eq. (36) changes as follows:

$$\omega_i^t = \frac{Q_i Q_j V_i}{R_i^3} \tag{37}$$

Now we can calculate the coordinates of particle based on angular frequency. Therefore, we first need to examine angular motion equation of particle in a magnetic field. In a simpler case, consider a particle with charge Q and mass m moving in a magnetic field with intensity B. If we consider angle between direction of motion of particle and direction of magnetic field as θ, final coordinates of particle are determined using Eq. (38):

$$X_i^t = R_{ij} \times \sin(\omega_i t) \tag{38}$$

where X_i^t is the i^{th} vector of particle coordinates in the t^{th} iteration, R_{ij} is the distance between two particles, and ω_i is the angular frequency of the particle vector, respectively.

The main step of this algorithm is developed using Eq. (39), with the help of the inverse Lorentz transformations and two phenomena of the length contraction and time dilation:

$$X_{new}^t = \beta^2 X_{old}^t + \left[\mu \frac{Q_i Q_j}{m r_{ij}^2} V_j\right]\sqrt{1-\beta^2} + X_2\sqrt{1-\beta^2} \tag{39}$$

where X_{new}^t is value of the path traversed by the particles in each iteration; μ is Lorentz force constant, and β is parameter representing the ratio of the velocity of the particle to the speed of light.

***Comparison Criterion*:** At each step, we calculate the objective function for the current point $X_{current}$ and the next point X_{next}, and compare them. If objective function for X_{next} is better than that for $X_{current}$, we set X_{next} as the new $X_{current}$ and continue the process. Otherwise, we search for a new point.

4. Hill-Climbing (HC) Algorithm

Hill-climbing (HC) algorithm is a mathematical optimization method used to find the optimal values of an objective function in the search space. In this algorithm, a point from search space is selected as starting point, and then by moving towards improved points, it tries to find the optimal point. The process of HC algorithm can be described as follows:

1) ***Starting point*:** A random point from search space is selected as starting point using Eq. (40):

$$X_{initial} = X_0 \tag{40}$$

2) ***Objective function evaluation*:** objective function is calculated at starting point and considered as current optimal value as:

$$f_{current} = f(X_{initial}) \tag{41}$$

3) ***Searching around the current point*:** By moving around starting point, objective function at surrounding points is calculated, and the point with a better value is selected as new point.
   - Improve the current point:

$$X_{new} = X_{initial} + \delta \tag{42}$$

where δ is a small value that can be positive or negative.

- Calculate the objective function at new point:

$$f_{new} = f(X_{new}) \tag{43}$$

4) ***Updating the position of the optimal responses:*** This process continues by repeating steps 2 and 3 until a specific termination condition is met, for example, until reaching a maximum number of steps or until the change in the value of the objective function reaches a minimum amount.

$$\text{if}\left[\begin{matrix} \left|f_{new} - f_{current}\right| < \text{thredshol} \\ f_{new} < f_{current} \end{matrix}\right. \Rightarrow \left|\begin{matrix} X = X_{new} \\ \text{and} \\ f_{current} = f_{new} \end{matrix}\right. \tag{44}$$

5) ***Obtaining the optimal point:*** The point with the best objective function obtained at the end of the process is selected as the optimal point.

This algorithm is applied as a simple and effective method for optimization, especially in cases where the objective function does not have the ability to directly calculate its derivatives, or the search is performed in a complex feasible space. The search process and convergence of the HC algorithm are shown in Fig. 3.

5. The SRS Algorithm based on HC Algorithm

Improving the local search engines is one of the most important steps in enhancing the performance and accuracy of the algorithms. Evolutionary algorithms often face complex problems, such as optimization, while seeking the optimal point in the search space. These algorithms typically utilize local search engines to navigate the search space. Strengthening these local search engines can significantly impact the effectiveness and efficiency of evolutionary algorithms. In this study, HC algorithm is employed to enhance local search engines. These two algorithms are utilized independently in various optimization and search problem domains. These methods strive to enhance local search mechanism by incorporating local information from objective function and moving in an ascending direction within search space.

In addition, the mutual improvement methods can be used among local search engines. For instance, various local search engines can be employed, and information can be exchanged between them to efficiently find optimal points and reduce the likelihood of getting stuck in local minima. Furthermore, the utilization of diversity-enhancing methods can enhance the strength of local search engines. By incorporating random or diverse elements into the search process, the chances of getting stuck in local minima decrease, and the algorithm promptly progresses towards optimal points. Overall, strengthening local search engines is a fundamental aspect in improving the performance and accuracy of metaheuristic algorithms. The use of local optimization methods, mutual enhancement between different search engines, and the use of diversity enhancement methods can lead to significant improvements in the efficiency of these algorithms.

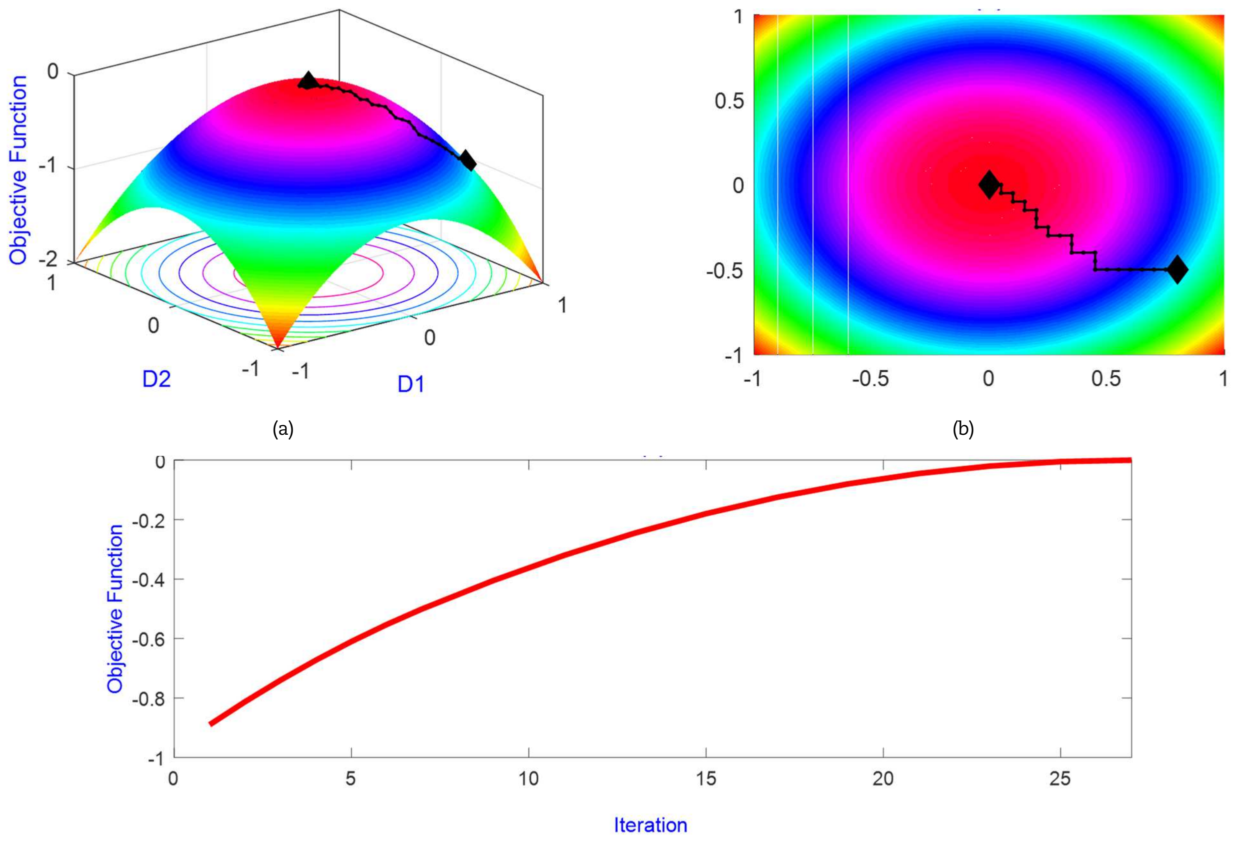

Fig. 3. (a) 3D view of climbing, (b) 2D view of climbing process, (c) Convergence history to the peak point.

```
MATLAB pseudo-code of SRSHC algorithm
% Initialize parameters
SRS_params = ...           % Set SRS-specific parameters
HC_params = ...            % Set HC-specific parameters
% Initialize population randomly within bounds
population = initialize_population(populationSize);
% Evaluate initial fitness of population
fitness = evaluate_fitness(population);
% Main optimization loop
for iter = 1:maxIterations
    % ------ SRS Phase: Global Exploration ------
    for i = 1:populationSize
        % Generate new position based on SRS principles
        newPosition = SRS_update(population(i), SRS_params);
        % Calculate fitness of new position
        newFitness = evaluate_fitness(newPosition);
        % Update position if new fitness is better
        if newFitness > fitness(i)
            population(i) = newPosition;
            fitness(i) = newFitness;
        end
    end
    % ------ HC Phase: Local Exploitation ------
    for i = 1:populationSize
        % Start from the current position from SRS phase
        currentPos = population(i);
        % Apply HC local search and refine solution
        refinedPosition = HC_refine(currentPos, HC_params);
        % Calculate fitness of refined position
        refinedFitness = evaluate_fitness(refinedPosition);
        % Update position if HC finds a better solution
        if refinedFitness > fitness(i)
            population(i) = refinedPosition;
            fitness(i) = refinedFitness;
        end
    end
    % Update the overall best solution if improved
    [maxFitness, bestIndex] = max(fitness);
    if maxFitness > bestSolution
        bestSolution = maxFitness;
        bestPosition = population(bestIndex);
    end
    % Check convergence
    if abs(maxFitness - bestSolution) < convergenceThreshold
       disp('Convergence reached');
        break;
    end
end
% Output final optimized solution
disp('Best Solution Found:');
disp(bestPosition);
```

By employing HC algorithm as a local search algorithm, performance of SRS algorithm has significantly improved. After determining the new positions of particles in the SRS algorithm, this vector is defined as the starting point of the HC algorithm. $X_{initial} = X_{SRS}$ is defined as the starting point of HC algorithm. Then, objective function value is evaluated, $f(X_{current}) = f(X_{initial})$. Then, steps 2 and 3 of HC algorithm are repeated until a certain condition is met. Then, in section 4, objective function values are updated. If optimal conditions are met, the optimal solution is displayed as output in section 5. Now, we evaluate optimal solutions of SRS and HC algorithms. If any changes have occurred, we use the solutions of HC algorithm to continue the optimization process and update the values of particle positions and the objective function; otherwise, we utilize the solutions of SRS algorithm.

SRS algorithm examines the global information in the search space, while HC algorithm utilizes local information. The combination of these two algorithms can exploit global and local information simultaneously, helping to improve search performance. SRS algorithm aims for extensive exploration in the search space, whereas HC algorithm focuses on leveraging local information. The combination of these two algorithms demonstrates a balance between exploration and exploitation, seeking to enhance the overall performance of the algorithm. The flow chart of novel approach is shown in Fig. 4.

6. Optimization Problem

Fundamental frequency has an essential role in the engineering applications because it affects the resonance behavior of the structures. As stiffened piezolaminated plates are generally subjected to low-frequency excitations under static and dynamic loads, resonance effect of the structure needs to be optimized by maximizing fundamental frequency of stiffened piezolaminated plates. Therefore, in this paper, an optimization model is improved, aiming to maximize the fundamental frequency. In this model, the design variables include the fiber orientations in the layers. The optimization problems can be formulated as:

$$\begin{aligned} &\text{Maximize } \omega \\ &\text{Subject to } -90^\circ \le \theta_k \le 90^\circ \quad k = 1,2,\ldots,N_{optimum} \end{aligned} \tag{45}$$

where, ω is fundamental frequency and θ are integer design variables of fiber orientation angles (which are varied from -90° to 90°) in the layers. In order to solve the above optimization problem, in this current study, a SRSHC algorithm is applied.

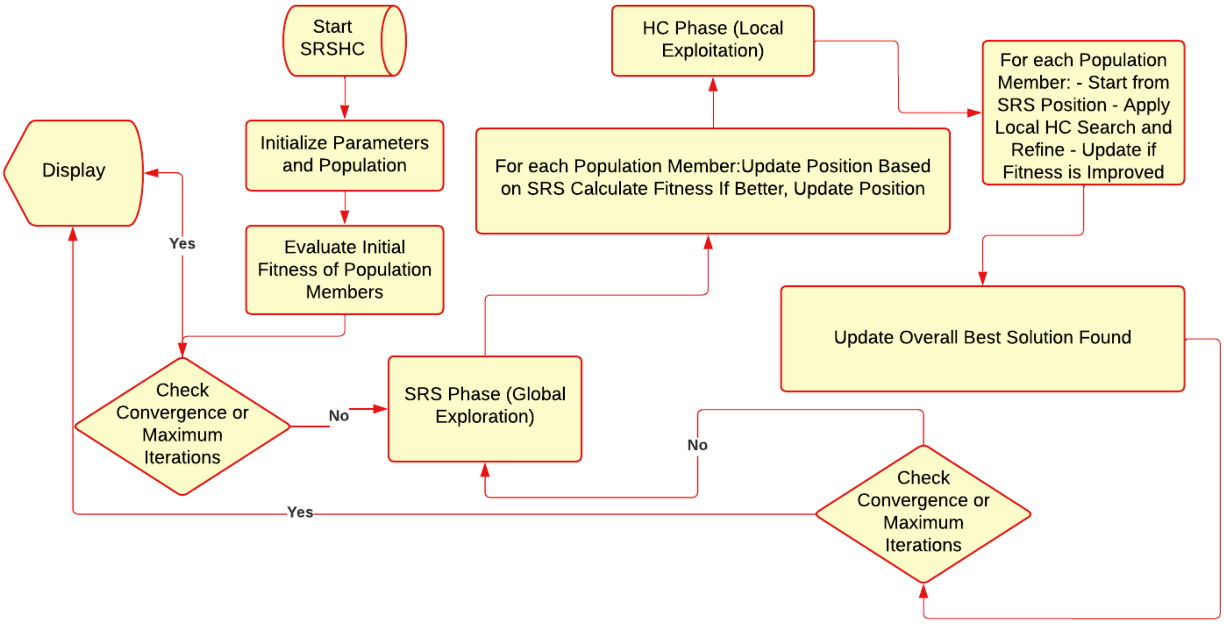

Fig. 4. Flow chart of SRSHC.

7. Numerical Results and Discussion

7.1. Validation of the present study

In this section, we first provide a variety of numerical examples to evaluate the versatility and applicability of the present study, benchmarking our results against those found in the existing literature. For the free vibration analysis, we focus on simply supported square 6-layered piezoelectric laminated composite plates with two specific fiber orientation configurations: [p/0/90/90/0/p] and [p/45/-45/-45/45/p], both without stiffeners. In these configurations, each piezoelectric layer has a thickness of $0.1h$, and each elastic layer has a thickness of $0.2h$, with the stiffness factor $V_a = 0$ set to zero. The material properties used for this analysis are listed in Table 1, and all layers are assumed to have a unit density $\rho = 1\ kg/m^3$.

As demonstrated in Table 2, the results obtained from the present study show good agreement with those reported in the literature, underscoring the accuracy and reliability of our approach. The comparison highlights the model's capacity to predict the free vibration characteristics of piezoelectric laminated composites accurately, which is essential for validating the approach used in this study and confirming its applicability to similar structural configurations. This agreement also illustrates that our simplified model is effective for analyzing composite structures with different fiber orientations, providing a robust basis for further research in this area.

Table 1. Material properties of composite and piezoelectric materials.

Properties	Graphite/Epoxy (Gr/Ep)	PZT-4
Elastic properties		
E_{11} (GPa)	132.38	81.3
E_{12} (GPa)	10.756	81.3
G_{12} (GPa)	5.654	30.6
ν_{12}	0.24	0.329
Piezoelectric coefficients		
$d_{31} = d_{32}$ (m/V)	-	-1.23e-10

Table 2. Comparison of frequency for a simply supported piezolaminated plate without stiffener ($b/h = 50$, $V_a = 0$).

	Lay-ups	$\omega_1/100$ in radians per second
Akhras and Li [13] (Elastic solution)	[p/0/90/90/0/p]	584.36
Akhras and Li [13] (Closed-circuit)		584.51
Akhras and Li [13] (Open-Circuit-C)		606.18
Akhras and Li [13] (Open-Circuit-N)		617.20
Present study		587.0295
Akhras and Li [13] (Elastic solution)	[p/45/-45/-45/45/p]	635.61
Akhras and Li [13] (Closed-circuit)		635.75
Akhras and Li [13] (Open-Circuit-C)		655.32
Akhras and Li [13] (Open-Circuit-N)		666.80
Present study		639.1756

Table 3. Results of the sensitivity analysis of the SRSHC algorithm.

Parameters	Best	Mean	Worst	Median	SD	Friedman Test	
						Mean rank	Best Rank
N=30, It.=100	1122925.8369	2015.1428747	1139738.405226	1140594.9039	1139775.855800	5.58	12
N=40, It.=100	1135260.0244	552.5782891	1140018.345931	1140590.5538	1140130.307900	3.32	6
N=50, It.=100	1138275.7627	417.7108232	1140260.701298	1140594.2296	1140459.944500	5.48	3
N=60, It.=100	1140331.7371	95.7605467	1140519.068950	1140594.8667	1140552.736100	10.05	1
N=30, It.=200	1138239.2591	493.4378639	1140365.627341	1140584.1540	1140491.872500	6.16	4
N=40, It.=200	1139554.7271	111.2822092	1140553.840743	1140594.3442	1140594.344200	10.80	2
N=50, It.=200	1138239.2591	493.4378639	1140365.627341	1140584.1540	1140491.872500	6.16	5
N=60, It.=200	1130951.4001	1341.7888046	1140271.390435	1140509.7208	1140509.720800	6.93	9
N=30, It.=300	1134520.9349	1402.8769866	1140005.562310	1140586.0162	1140366.848700	4.10	10
N=40, It.=300	1131197.5793	1608.9581412	1139802.494086	1140594.6038	1140573.833800	6.98	11
N=50, It.=300	1132276.2381	1130.0096061	1140053.561157	1140589.5640	1140126.055800	5.83	7
N=60, It.=300	1134978.2728	1293.0688007	1140102.776889	1140526.0318	1140496.697800	6.61	8

7.2. Optimal design problems

Since this problem is new and has not been optimized yet, it is necessary to perform a sensitivity analysis to achieve reliable results with the proposed optimization algorithm. This analysis controls the effect of the intrinsic parameters of SRSHC algorithm. A statistical significance test is applied to explore the result of the simulations. In this study, Friedman's statistical test is used. The results of SRSHC algorithm with different parameters are presented in Table 1 for simply supported 6-layered symmetric square piezolaminated plates without grid (V_a = 0). The material properties of composite are E_{11} = 181 GPa, E_{12} = 10.3 GPa, G_{12} = 7.17 GPa and V_{12} = 0.28. The material property of grid stiffener is E = 70 GPa. For each optimization case, 20 independent runs are performed. According to these results, the population size and maximum iteration are considered as 60 and 100, respectively. The convergence history for different tuning parameters is illustrated in Fig. 5.

The non-dimensional fundamental frequency is calculated as follows:

$$\bar{\omega} = \omega \frac{a^2}{h}\sqrt{\frac{\rho}{E_2}} \tag{46}$$

First, this optimization study investigates the comparison of optimum results for SRS and SRSHC algorithms for 10-layered symmetric square piezolaminated plates with iso grid 1 for different boundary conditions (ϕ = 0, V_a = 100). Optimum results of the six mixed boundary conditions as SSSS, CCCC, CSCS, CFCF, SFSF and CFFF are evaluated. It should be mentioned that the following data is used for different types of simply supported, clamped and free boundary conditions in edge i (i = 1,2,3,4):

$$\begin{aligned} &\text{Simply supported (S)}: k_i^l = 10^{10}, k_i^r = 0 \\ &\text{Clamped (C)}: k_i^l = 10^{10}, k_i^r = 10^{10} \\ &\text{Free }(F): k_i^l = 0, k_i^r = 0 \end{aligned} \tag{47}$$

As seen from Table 4, SRSHC algorithm has better optimum results than those of SRS algorithm. Also, it can be observed that the optimum fundamental frequency is decreased substantially with free edge condition, while it is increased by applying clamped mixed edge condition. Convergence history for different tuning parameters is illustrated in Fig. 6.

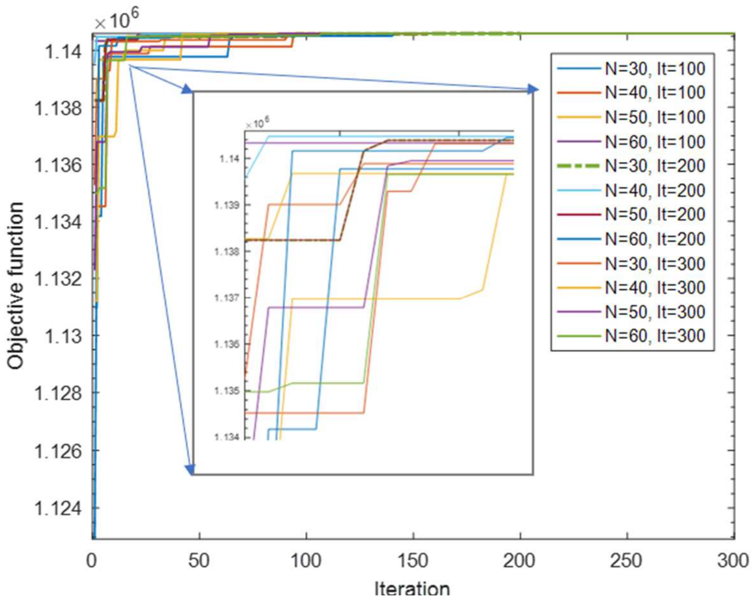

Fig. 5. Convergence history for different tuning parameters.

Table 4. Comparison of optimum results for SRS and SASHC algorithms for 10-layered symmetric square piezolaminated plates with iso grid 1 for different boundary conditions.

Boundary condition	SRS		SRSHC	
	Optimum stacking sequence	$\bar{\omega}$	Optimum stacking sequence	$\bar{\omega}$
SSSS	[p/43/-45/49/-49]s	4334.20	[p/44/-43/-46/45]s	4364.60
CCCC	[p/90/90/-90/-90]s	12842.09	[p/0/90/-90/90]s	12851.00
CSCS	[p/2/10/2/7]s	10502.54	[p/0/0/0/0]s	10568.00
CFCF	[p/0/1/4/9]s	8698.59	[p/0/0/0/0]s	8744.40
SFSF	[p/6/0/11/-4]s	1656.73	[p/0/0/0/0]s	1686.00
CFFF	[p/5/3/4/1]s	212.64	[p/0/0/0/0]s	215.71

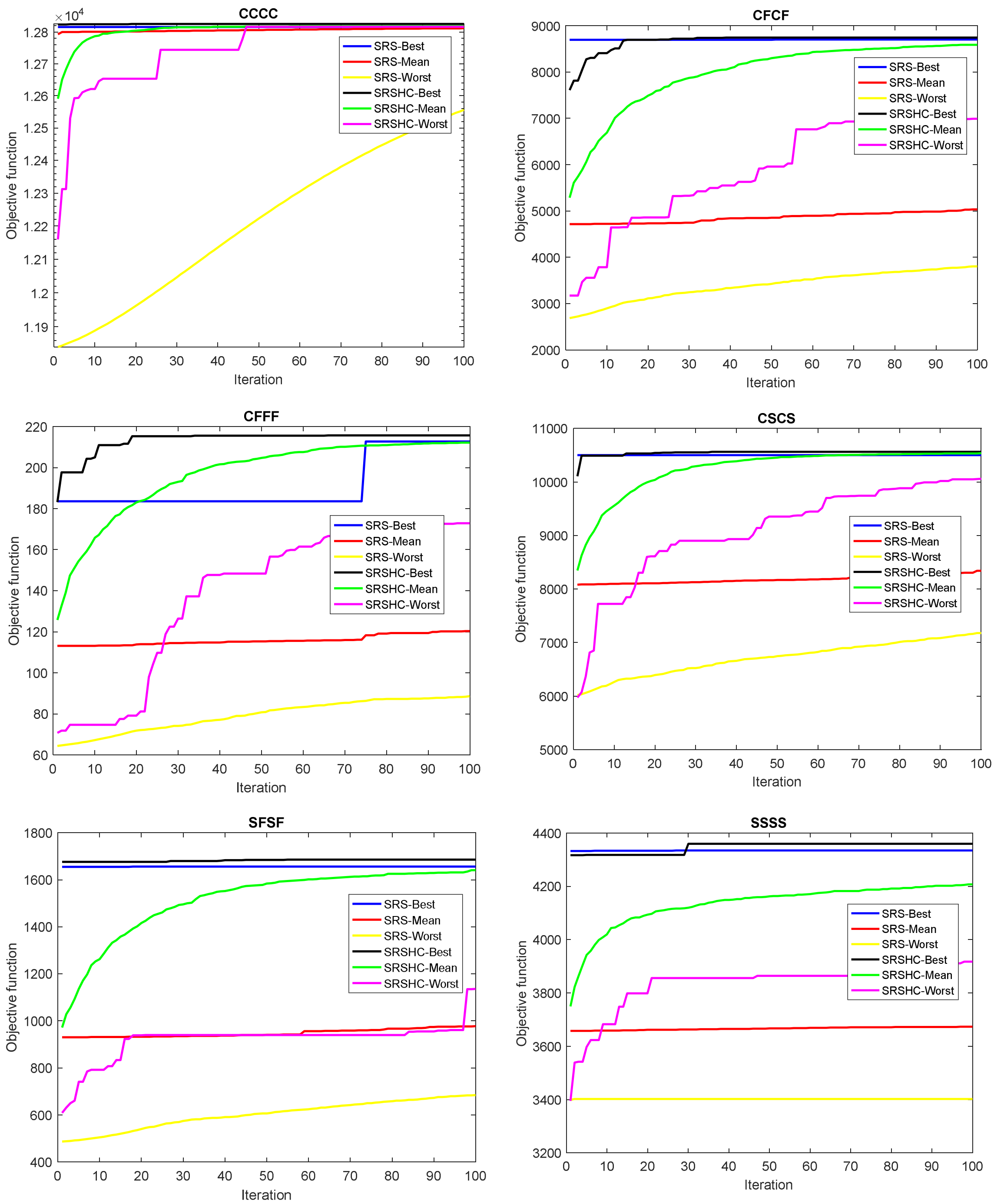

Fig. 6. Convergence histories for SRS and SRSHC algorithms.

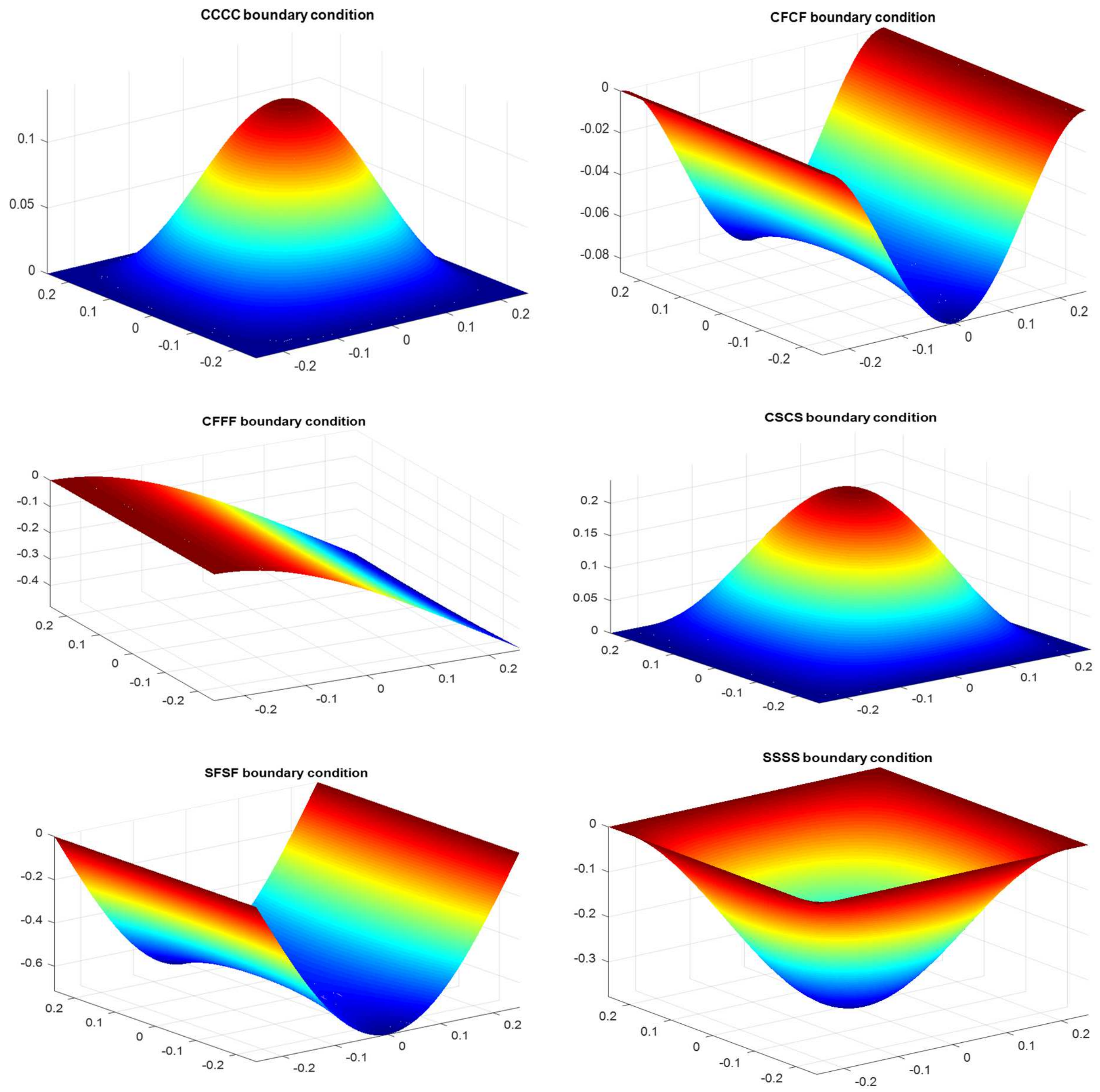

Fig. 7. Mode shapes of different boundary conditions.

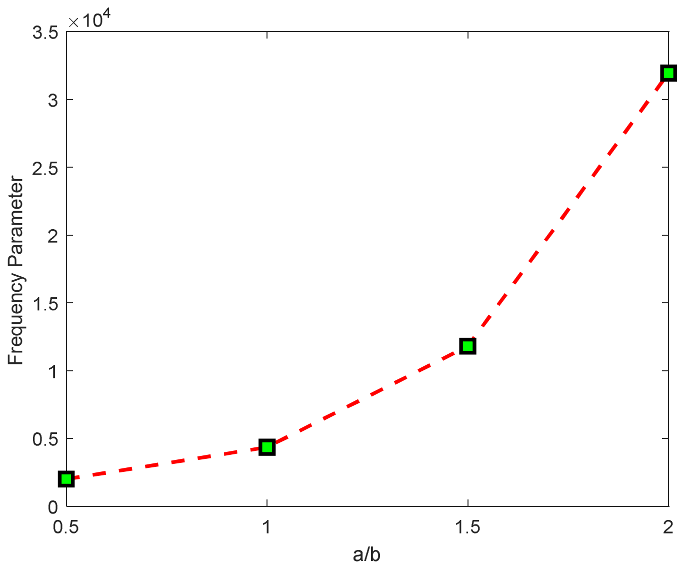

Fig. 8. Effect of a/b ratio on the fundamental frequency.

Table 5. Effect of *a/b* ratio on the optimum fiber orientations.

a/b	Optimum stacking sequence
0.5	[p/0/0/0/0]s
1	[p/45/-47/-45/48]s
1.5	[p/63/-63/-59/68]s
2	[p/-90/-90/90/90]s

Table 6. Effect of different grid shapes on the optimum results.

Grid shapes	Optimum stacking sequence	$\bar{\omega}$
Angle grid	[p/45/-44/-48/43]s	4359.00
Iso grid 1	[p/46/-44/-44/48]s	4364.50
Iso grid 2	[p/47/-46/-43/40]s	4360.20
Ortho grid	[p/47/-46/-43/40]s	4360.20
Orthotropic grid	[p/47/-46/-45/44]s	4369.00

Table 7. Effect of angle of diagonal ribs on the optimum fiber orientations.

ϕ	Optimum stacking sequence
0	[p/46/-45/-45/45]s
15	[p/44/-46/-43/47]s
30	[p/47/-46/-45/44]s
45	[p/46/-45/-45/45]s
60	[p/46/-46/-42/47]s
75	[p/43/-46/-44/47]s
90	[p/46/-44/-49/45]s

The vibration modes of a 10-layered symmetric square piezolaminated plates under various boundary conditions significantly affect its dynamic behavior (Fig. 7). These modes have been extracted for the optimized results presented in Table 4. Under the CCCC boundary condition, the vibration modes appear as constrained bending due to the high stiffness at the edges. Under the CFCF condition, the modes exhibit a combination of bending and localized deflection. In the CFFF condition, the modes display dominant bending along the free edges with minimal deformation near the clamped edge. For the CSCS condition, the modes combine bending behavior with linear deformation at the simply supported edges. Under the SFSF condition, the mode shapes are characterized by significant deformations at the free edges. Finally, under the SSSS condition, the vibration modes exhibit maximum flexibility with bending behavior and uniform deformation along all edges. This analysis highlights the critical influence of boundary conditions on the mode shapes and overall structural behavior, with an emphasis on the optimized results in Table 4.

The effect of different plate aspect ratios (*a/b*) on the optimum results is studied for simply supported 10-layered symmetric piezolaminated plates with iso grid 2 (ϕ = 0, V_a = -100). As seen from Fig. 8, the non-dimensional fundamental frequencies increase with the increase in aspect ratio. It can be also observed that non-dimensional fundamental frequency increases slowly for small aspect ratio ($a/b \leq 1$) and then rapidly increases with increasing aspect ratio. However, as seen from Table 5, different *a/b* ratio has a substantial effect on the optimum fiber orientations.

The effect of different grid shapes on the optimum results is studied for simply supported 10-layered symmetric square piezolaminated plates (ϕ = 0, V_a = 200). As seen from Table 6, the non-dimensional fundamental frequency of the piezolaminated plate with an orthotropic grid is the largest due to the high stiffness of the grid components. On the other hand, piezolaminated plate with an angle grid has the smallest fundamental frequency. However, different grid shape has a little effect on the optimum fiber orientations.

Figure 9 shows the effect of different angle of diagonal ribs (ϕ) on the fundamental frequency for simply supported 10-layered symmetric square piezolaminated plates with an orthotropic grid. (V_a = -200). As seen, the non-dimensional maximum fundamental frequency occurs for ϕ = 45°. After that, the non-dimensional fundamental frequency decreases with increasing angle of diagonal ribs. As observed, the non-dimensional minimum fundamental frequency occurs for ϕ = 90°. On the other hand, as seen from Table 7, different angle of diagonal ribs has no substantial effect on the optimum fiber orientations.

8. Conclusion

In this study, the optimization of the fundamental frequency of stiffened piezolaminated symmetric composite plates was investigated using the Special Relativity Search based on Hill Climbing (SRSHC) algorithm. The main focus was on determining the optimal fiber orientations to maximize the fundamental frequency, considering various factors such as boundary conditions, grid shapes, and plate aspect ratios. The conclusions drawn from the optimization results provide valuable insights into the behavior of these composite plates under different configurations. In the following, the key findings and contributions of this study are summarized.

1) This study presents an optimization approach for maximizing the fundamental frequency of stiffened piezolaminated symmetric composite plates using the Special Relativity Search based on Hill Climbing (SRSHC) algorithm. The optimization focuses on determining the optimal fiber orientations while considering various parameters, including boundary conditions, grid shapes, and aspect ratios.

2) The formulation of the study is based on the Classical Laminate Plate Theory (CLPT), and all results are limited to thin plates to avoid shear effects. The analysis shows that the fundamental frequency of piezolaminated plates with an orthotropic grid is the highest, due to the superior stiffness properties of the grid material.

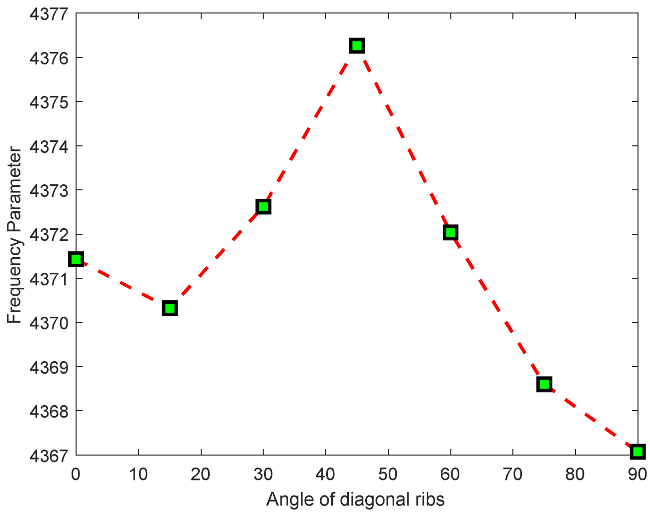

Fig. 9. Effect of angle of diagonal ribs on the fundamental frequency.

3) On the other hand, piezolaminated plates with an angled grid exhibit the lowest fundamental frequency. However, the shape of the grid has minimal influence on the optimal fiber orientations, with the maximum fundamental frequency occurring at a fiber orientation of $\phi = 45°$. Increasing the angle of the diagonal ribs reduces the fundamental frequency.

4) The minimum fundamental frequency is observed when the fiber orientation is $\phi = 90°$. Interestingly, the angle of the diagonal ribs has little effect on the optimal fiber orientations, suggesting that the rib angle mainly influences the overall frequency without significantly altering the optimal fiber alignment.

5) A comparison between the SRSHC and the SRS optimization algorithms demonstrates that the SRSHC algorithm outperforms the SRS algorithm in terms of robustness and optimization efficiency. This proves the effectiveness and excellence of the SRSHC algorithm in solving complex optimization problems related to composite plate design.

Author Contributions

V. Goodarzimehr designed the study and developed the methodology. U. Topal and M. Bohlooly Fotovat conducted data analysis and simulation. All authors contributed to writing and editing the manuscript. The manuscript was written through the contribution of all authors. All authors discussed the results, reviewed, and approved the final version of the manuscript.

Acknowledgments

Not applicable.

Conflict of Interest

The authors declared no potential conflicts of interest concerning the research, authorship, and publication of this article.

Funding

The authors received no financial support for the research, authorship, and publication of this article.

Data Availability Statements

The datasets generated and/or analyzed during the current study are available from the corresponding author on reasonable request.

References

[1] Jayakumar, K., Yadav, D., Rao, B.N., Nonlinear free vibration analysis of simply supported piezo-laminated plates with random actuation electric potential difference and material properties, *Communications in Nonlinear Science and Numerical Simulation*, 14, 2009, 1646–1663.
[2] Panda, S., Ray, M.C., Active control of geometrically nonlinear vibrations of functionally graded laminated composite plates using piezoelectric fiber reinforced composites, *Journal of Sound and Vibration*, 325, 2009, 186–205.
[3] Dash, P., Singh, B.N., Nonlinear free vibration of piezoelectric laminated composite plate, *Finite Elements in Analysis and Design*, 45, 2009, 686-694.
[4] Dash, P., Singh, B.N., Geometrically nonlinear free vibration of laminated composite plate embedded with piezoelectric layers having uncertain material properties, *Journal of Vibration and Acoustics*, 134, 2012, 1–13.
[5] Huang, X.L., Shen, H.S., Nonlinear free and forced vibration of simply supported shear deformable laminated plates with piezoelectric actuators, *International Journal of Mechanical Sciences*, 47, 2005, 187–208.
[6] Deepak, P., Jayakumar, K., Panda, S., Nonlinear free vibration analysis of piezoelectric laminated plate with random actuation electric potential difference and thermal loading, *Applied Mathematical Modelling*, 95, 2021, 74–88.
[7] Zhang, Y.F., Zhanga, W., Yao, Z.G., Analysis on nonlinear vibrations near internal resonances of a composite laminated piezoelectric rectangular plate, *Engineering Structures*, 173, 2018, 89-106.
[8] Moita, J.M.S., Soares, C.M.M., Soares, C.A.M., Geometrically non-linear analysis of composite structures with integrated piezoelectric sensors and actuators, *Composite Structures*, 57, 2002, 253–261.
[9] Krommer, M., Piezoelastic vibrations of composite Reissner–Mindlin-type plates, *Journal of Sound and Vibration*, 263, 2003, 871–891.
[10] Shu, X., Free vibration of laminated piezoelectric composite plates based on an accurate theory, *Composite Structures*, 67, 2005, 375–382.
[11] Pietrzakowski, M., Piezoelectric control of composite plate vibration: Effect of electric potential distribution, *Computers and Structures*, 86, 2008, 948–

954.
[12] Milazzo, A., Orlando, C., An equivalent single-layer approach for free vibration analysis of smart laminated thick composite plates, *Smart Materials and Structures*, 21, 2012, 075031.
[13] Akhras, G., Li, W., Stability and free vibration analysis of thick piezoelectric composite plates using spline finite strip method, *International Journal of Mechanical Sciences*, 53, 2011, 575-584.
[14] Torres, D.A.F., Mendonça, P.T.R., HSDT-layerwise analytical solution for rectangular piezoelectric laminated plates, *Composite Structures*, 92, 2010; 1763–1774.
[15] Topdar, P., Sheikha, A.H., Dhang, N., Vibration characteristics of composite/sandwich laminates with piezoelectric layers using a refined hybrid plate model, *International Journal of Mechanical Sciences*, 49, 2007, 1193–1203.
[16] Loja, M.A.R., Barbosa, J.I., Soares, C.M.M., Soares, C.A.M., Analysis of piezolaminated plates by the spline finite strip method, *Computers and Structures*, 79, 2001, 2321-2333.
[17] Chanda, A.G., Kontoni, D.P.N., Sahoo, R., Development of analytical and FEM solutions for static and dynamic analysis of smart piezoelectric laminated composite plates on elastic foundation, *Journal of Engineering Mathematics*, 138, 2023, 1-54.
[18] Robaldo, A., Carrera, E., Benjeddou, A., A unified formulation for finite element analysis of piezoelectric adaptive plates, *Computers and Structures*, 84, 2006, 1494–1505.
[19] Tanzadeh, H., Amoushahi, H., Buckling and free vibration analysis of piezoelectric laminated composite plates using various plate deformation theories, *European Journal of Mechanics-A/Solids*, 74, 2019, 242-256.
[20] Zhang, Z., Feng, C., Liew, K.M., Three-dimensional vibration analysis of multilayered piezoelectric composite plates, *International Journal of Engineering Science*, 44, 2006, 397–408.
[21] Phung-Van, P., Lorenzis, L.D., Thai, C.H., Abdel-Wahab, M., Nguyen-Xuan, H., Analysis of laminated composite plates integrated with piezoelectric sensors and actuators using higher-order shear deformation theory and isogeometric finite elements, *Computational Materials Science*, 96, 2015, 495–505.
[22] Jiang, Y., Zhang, W., Zhang, Y.F., Lu, S.F., Nonlinear vibrations of four-degrees of freedom for piezoelectric functionally graded graphene-reinforced laminated composite cantilever rectangular plate with PPF control strategy, *Thin-Walled Structures*, 188, 2023, 110830.
[23] Lu, S.F., Jiang, Y., Zhang, W., Song, X.J., Vibration suppression of cantilevered piezoelectric laminated composite rectangular plate subjected to aerodynamic force in hygrothermal environment, *European Journal of Mechanics - A/Solids*, 83, 2020, 104002.
[24] Talebitooti, R., Daneshjoo, K., Jafari, S.A.M., Optimal control of laminated plate integrated with piezoelectric sensor and actuator considering TSDT and meshfree method, *European Journal of Mechanics-A/Solids*, 55, 2016, 199-211.
[25] Oh, I., Han, J., Lee, I., Postbuckling and vibration characteristics of piezolaminated composite plate subject to thermo-piezoelectric loads, *Journal of Sound and Vibration*, 233, 2000, 19-40.
[26] Donadon, M.V., Almeida, S.F.M., de Faria, A.R., Stiffening effects on the natural frequencies of laminated plates with piezoelectric actuators, *Composites Part B: Engineering*, 33, 2002, 335–342.
[27] Momeni, M., Fallah, N., Meshfree finite volume method for active vibration control of temperature-dependent piezoelectric laminated composite plates, *Engineering Analysis with Boundary Elements*, 130, 2021, 364-378.
[28] Nguyen-Quang, K., Vo-Duy, T., Dang-Trunga, H., Nguyen-Thoi, T., An isogeometric approach for dynamic response of laminated FG-CNT reinforced composite plates integrated with piezoelectric layers, *Computer Methods in Applied Mechanics and Engineering*, 332, 2018, 25-46.
[29] Niu, B., Shan, Y., Lund, E., Discrete material optimization of vibrating composite plate and attached piezoelectric fiber composite patch, *Structural and Multidisciplinary Optimization*, 60, 2019, 1759–1782.
[30] Correia, V.M.F., Soares, C.M.M., Soares, C.A.M., Refined models for the optimal design of adaptive structures using simulated annealing, *Composite Structures*, 54, 2001, 161-167.
[31] Correia, V.M.F., Madeira, J.F.A., Araújo, A.L., Soares, C.M.M., Multiobjective design optimization of laminated composite plates with piezoelectric layers, *Composite Structures*, 169, 2017, 10–20.
[32] Padoin, E., Santos, I.F., Perondi, E.A., Menuzzi, O., Gonçalves, J.F., Topology optimization of piezoelectric macro-fiber composite patches on laminated plates for vibration suppression, *Structural and Multidisciplinary Optimization*, 59, 2019, 941–957.
[33] Alamir, A.E., Optimal control and design of composite laminated piezoelectric plates, *Smart Structures and Systems*, 15, 2015, 1177-1202.
[34] Li, J., Li, F., Narita, Y., Active control of thermal buckling and vibration for a sandwich composite laminated plate with piezoelectric fiber-reinforced composite actuator facesheets, *Journal of Sandwich Structures & Materials*, 21, 2019, 2563–2581.
[35] Goodarzimehr, V., Topal, U., Bohlooly, M., A novel approach for buckling optimization of stiffened piezolaminated composite plates, *Journal of Composite Materials*, 58, 2024, 2975-2991.
[36] Goodarzimehr, V., Topal, U., Vo-Duy, T., Shojaee, S., Improved chaos game optimization algorithm for optimal frequency prediction of variable stiffness curvilinear composite plate, *Journal of Reinforced Plastics and Composites*, 42(19-20), 2023, 1054-1066.
[37] Goodarzimehr, V., S. Shojaee, S. Talatahari, Hamzehei-Javaran, S., Generalized Displacement Control Analysis and Optimal Design of Geometrically Nonlinear Space Structures, *International Journal of Computational Methods*, 20 (07), 2022, 2143018.
[38] Goodarzimehr, V., Fazlı, M., Fanaie, N., Gandomi, A.H., Enhanced special relativity search algorithm based lorentz force for structural optimization, *International Journal of Computational Methods*, 2024, DOI: 10.1142/S0219876224500646.
[39] Goodarzimehr, V., Topal, U., Das, A.K., Vo-Duy, T., SABO algorithm for optimum design of truss structures with multiple frequency constraints, *Mechanics Based Design of Structures and Machines*, 52, 2024, 7745-7777.
[40] Omidinasab, F., Goodarzimehr, V., A hybrid particle swarm optimization and genetic algorithm for truss structures with discrete variables, *Journal of Applied and Computational Mechanics*, 6, 2020, 593-604.
[41] Zarzoor, A.K., Jaber, A.A., Shandookh, A.A., Structural optimization-based enhancement of the dynamic performance for horizontal axis wind turbine blade, *Journal of Applied and Computational Mechanics*, 2024, DOI: 10.22055/jacm.2024.47526.4734.
[42] Inman, D.J., Gunasekar, A., Frequency separation in architected structures using inverse methods, *Journal of Applied and Computational Mechanics*, 7, 2021, 2084-2095.
[43] Bohlooly, M., Malekzadeh, F.K., Buckling and postbuckling of concentrically stiffened piezo-composite plates on elastic foundations, *Journal of Applied and Computational Mechanics*, 5, 2019, 128-140.
[44] Bohlooly, M., Kouchakzadeh, M.A., Mirzavand, B., Noghabi, M., Dynamic instability characteristics of advanced grid stiffened conical shell with laminated composite skins, *Journal of Sound and Vibration*, 488, 2020, 115572.
[45] Kouchakzadeh, M.A., Rahgozar, M., Bohlooly, M., Buckling of laminated composite plates with elastically restrained boundary conditions, *Structural Engineering and Mechanics*, 74, 2020, 577-588.
[46] Permoon, M.R., Shakouri, M., Haddadpour, H., Free vibration analysis of sandwich conical shells with fractional viscoelastic core, *Composite Structures*, 214, 2019, 62-72.
[47] Goodarzimehr, V., Talatahari, S., Shojaee, S., Hamzehei-Javaran, S., Special relativity search for applied mechanics and engineering, *Computer Methods in Applied Mechanics and Engineering*, 403, 2023, 115734.
[48] Goodarzimehr, V., Shojaee, S., Hamzehei-Javaran, S., Talatahari, S., Special relativity search: A novel metaheuristic method based on special relativity physics, *Knowledge-Based Systems*, 57, 2022, 109484.

ORCID iD

Vahid Goodarzimehr https://orcid.org/0000-0001-6268-1890
Umut Topal https://orcid.org/0009-0006-0054-3154
Mehdi Bohlooly Fotovat https://orcid.org/0000-0001-7749-916X

How to cite this article: Goodarzimehr V., Topal U., Bohlooly Fotovat M. Optimal Frequency of Stiffened Piezolaminated Composite Plates Implementing a Hybrid Special Relativity Search and Hill Climbing Optimization Algorithm, *J. Appl. Comput. Mech.*, 11(4), 2025, 1022-1038. https://doi.org/10.22055/jacm.2024.47914.4837